

Large-Format, 6-10 and 10-15 micron Dual Broadband QWIP Focal Plane Arrays

S. V. Bandara, S. D. Gunapala, F. M. Reininger,
J. K. Liu, S. B. Rafol, J. M. Mumolo, D. Z. Ting and T. Q. Trinh,

Jet Propulsion Laboratory, California Institute of Technology
4800 Oak Grove Drive, Pasadena, CA 91109

ABSTRACT

The Jet Propulsion Laboratory (JPL) is developing a 512×640-format, dual broadband, Quantum Well Infrared Photodetector (QWIP) focal plane array (FPA) for an imaging interferometer. This is a new type of imaging interferometer which is based on special Fourier-transform spectroscopy, scans interferograms digitally without moving any optical components. It is stable enough to measure fluctuating target signatures from unstable platforms, making it ideal for detecting chemical agents from a remotely piloted aircraft. These static interferometers require large-format FPAs with high uniformity and operability. QWIP technology is ideal for this instrument because it has achieved remarkable success in advancing highly uniform, highly-operability, and large-format multicolor FPAs. The FPA used in the interferometer covers the wavelength from 6-10 μm and 10-15 μm in alternative rows.

Key words: Infrared imaging, quantum well, interferometer, chemical detection

1. INTRODUCTION

Infrared spectroscopy is rapidly becoming the most accurate and reliable technique for remotely identifying various species of gases. Infrared photons can excite rotational and vibrational modes of molecules, generating absorption or emission bands in the infrared spectrum. The shape and location of these bands uniquely identify the molecules that constitute the volume of gas or atmosphere being investigated. The gas abundances are determined by performing an atmospheric retrieval on the measured radiance data from a remote sensing spectrometer. Retrievals are essentially comparisons of the measurements to atmospheric simulation models. A nadir viewing sounder must also determine the ground temperature so that the background can be removed. Unfortunately, it is difficult to accurately determine ground temperature and spectral-emissivity in real time to perform a background removal without distorting the vapor spectra. Also, the computational burden of performing the large matrix inversions for retrievals is too great for real-time analysis on a small platform.

A miniature interferometer that can perform automated detection in the interferogram domain has been developed at the Jet Propulsion Laboratory (JPL). This interferometer, known as the spatially modulated prism interferometer (SMPI) [1,2], is a new type of imaging interferometer that has double the efficiency of conventional interferometers and only a fraction of the mass and volume. Its spectral resolution is independent of wavelength and slit width, an attribute made possible by generating interferograms at a pupil plane. The SMPI uses digital signal processing techniques to isolate the narrowband vapor spectra from the broadband surface spectra. It should then be possible to identify the presence of a predetermined set of chemicals or indicate the presence of "unknown" chemicals. The more complex poisonous gases tend to have their spectral signatures in the middle- and long-wavelength infrared (MWIR and LWIR) regimes. The energy source can be the ground or the gas itself where the peak of its Planck energy distribution will occur between 9 and 11 μm if the temperature is between 300 and 270 K. Therefore, an imaging spectrometer with its 6-15 μm spectrum centered at 10 μm would be ideal because it will most likely encompass the spectral signatures of all possible chemical agents.

The high-resolution SMPI requires a small-pixel, large-format focal plane array (FPA) with high uniformity and operability [1,2]. It would also be desirable to have low 1/f noise to reduce the calibration burden and increase the temporal stability. The GaAs/AlGaAs-based Quantum Well Infrared Photodetector (QWIP) is an ideal candidate for the development of such FPAs due to its mature fabrication technologies and inherent properties such as wavelength tailorability [3-5]. QWIP technology has shown remarkable success in advancing low-cost, highly uniform, high-

operability, large-format FPAs. It also permits vertical integration of multi-quantum well (MQW) stacks [6-8]. Each MQW stack absorbs photons within the specified wavelength band, allowing other photons to transmit through permitting multiband detection. The wavelength of the peak response and cutoff can be continuously tailored by varying layer thickness (well width), barrier composition (barrier height), and carrier density (well-doping density). The GaAs/Al_xGa_{1-x}As material system allows the quantum well parameters to be varied over a range wide enough to enable light detection at any wavelength range from 6 to 20 μm [3-8]. By adding a few monolayers of In_yGa_{1-y}As during the GaAs quantum well growth, the short wavelength limit can be extended to 3 μm [9]. The spectral bandwidth of these detectors can be tuned from narrow ($\Delta\lambda/\lambda \sim 10\%$) to wide ($\Delta\lambda/\lambda \sim 40\%$), according to application requirements [10].

This article includes a brief introduction to the miniature SMPI and mainly focuses on the dual-band QWIP FPA design, fabrication, characterization, and performance of individual detectors. A detailed description of the SMPI can be found in [1].

2. THE SMPI INSTRUMENT CONCEPT

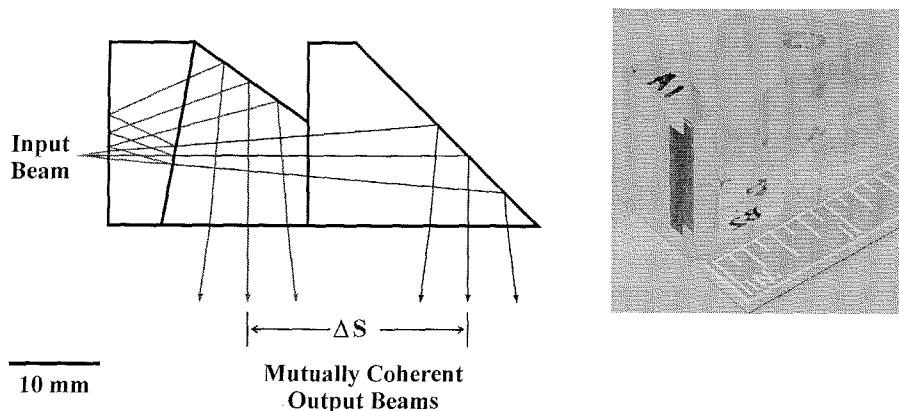


Figure 1: The beam-shearing prism generates mutually coherent beams [1].

The spatial modulation principle is based on famous Young's double slit experiment, in which a beam is widely separated into two mutually coherent halves that interfere in proportion to the path-length difference between their wavefronts. A three-mirror telescope focuses a beam into an image slit. A compact design form of the recently invented

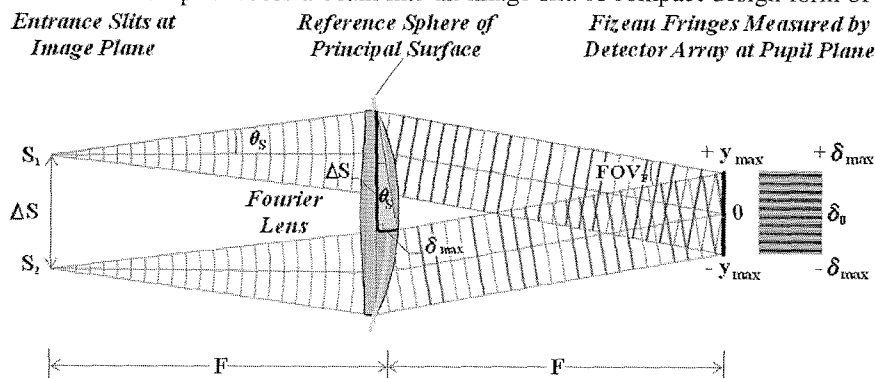


Figure 2: Generating static fringes at a pupil plane using a Fourier lens [1].

beam-shearing prism [1,2] splits the beam into two mutually coherent beams (see Figure 1). If the two beams are

spherical and telecentric when they enter the lens, they will exit collimated and converge at a pupil plane (see Figure 2). A QWIP array, positioned at the pupil plane, detects the resulting interference patterns. The beam-shearing prism consists of three separate potassium bromide prisms hard-mounted in an aluminum structure. The prism enables the detector array to use 100% of the input beam to maximize the signal-to-noise ratio. The lens is called a Fourier lens because it performs a special Fourier transformation of the image into a pupil. However, the Fourier optics is not telecentric in the image plane, so in the orthogonal direction, an image is generated.

This instrument can be used in a unmanned airborne vehicle (UAV), using a push-broom approach to remotely scan the atmosphere for poisonous gas clouds. The instrument would acquire a 25° swath of the atmosphere one line at a time in a direction perpendicular to the flight path. The instrument would be an imaging spectrometer that generates a spectral signature of the gas in each image pixel that contains the gas signature. It would not be necessary, or desirable, for the sensor to fly through the gas cloud to detect it. When the instrument is rotated 90 deg so that its field of view is in line with the vehicle's velocity vector, a side-scanning mirror scans the image line ± 75 deg on either side of the UAV to yield a sixfold increase in coverage. The most accurate method for determining atmospheric vapor content from a remote sensing spectrometer is to perform retrievals on the collected data. If the imaging spectrometer is actually an interferometer, then the first step is to Fourier-transform the interferogram associated with each instantaneous field of view (IFOV) of the image into radiance spectra. Though the results are reliable and accurate, large matrix inversions are required and the computational burden is too great for real-time analysis on a small UAV. Fortunately, detection of a gas does not necessarily require an accurate determination of its abundance or temperature at all altitudes. Since poisonous gases are not a natural part of the atmosphere, it would be sufficient to merely indicate their presence. As indicated in Figure 3, the interferogram automatically separates the narrowband features of the atmosphere from the broadband features of the surface. It should therefore be possible to use the interferogram directly to identify the gas without the computational burden of processing an atmospheric retrieval.

3. DETECTOR FOCAL PLANE ARRAY

A 640x512 format interlaced dual broadband QWIP FPA based on a GaAs/AlGaAs material system has been developed for the SMPI instrument. Two broadbands cover 6-10 μm and 10-15 μm wavelength ranges with minimum spectral overlap. The main benefit of two bands is it enables almost a doubling of the spectral resolution for the same

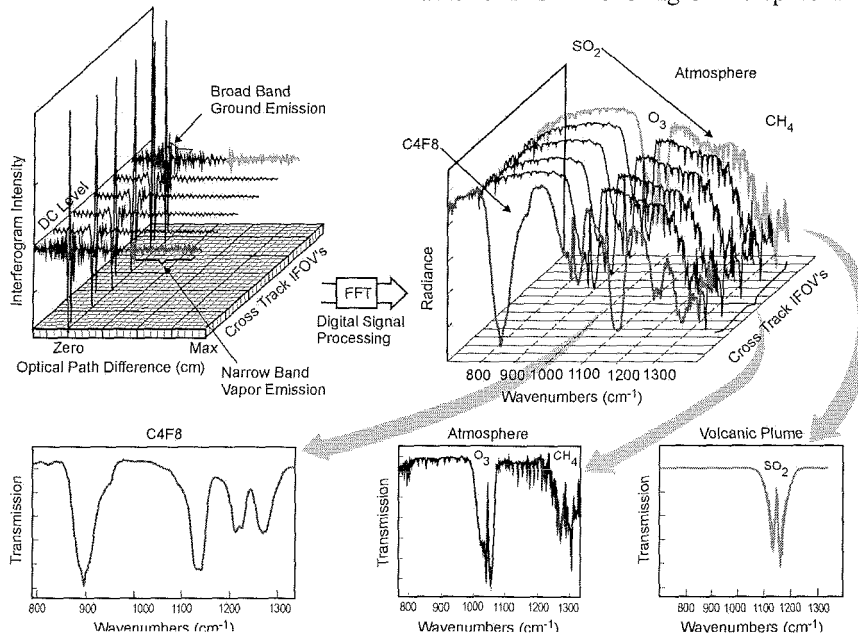


Figure 3: Generating transmission spectra from interferograms automatically separates the narrowband features of the atmosphere from the broadband features of the surface [1].

number of interferogram pixels (640). This is accomplished by Nyquist folding the 6-10 μm band about the 10 μm point

[1,2]. With one 6-15 μm band, the Nyquist folding point must be shifted out to 6 μm to prevent aliasing. Figure 4 shows a schematic diagram representing the dual band detector array. This FPA consists of two independently readable infrared (IR) bands covering 6-10 μm and 10-14 μm and each band occupies alternate rows (640 \times 256 pixel area) within the single imaging array. Optimized achromatic 2-D reflective gratings with deeper groove depths were utilized in this FPA in order to reflect light in preferred directions, allowing absorption within the active MQW layers of each IR band [8,11-14]. In addition to light coupling, these gratings serve as a contact to the active stack while shorting the unwanted stacks [8]. During the fabrication of detector arrays, individual pixels were defined by photolithographic processing techniques [5,6]. Two broadband detectors were defined by a deep trench etch process, and a detector short-circuiting process eliminated the unwanted spectral bands. As shown in Figure 4, the unwanted top detectors were electrically shorted by gold-coated reflective 2-D etch gratings. The unwanted bottom detectors were electrically shorted through the column from outside the array [8].

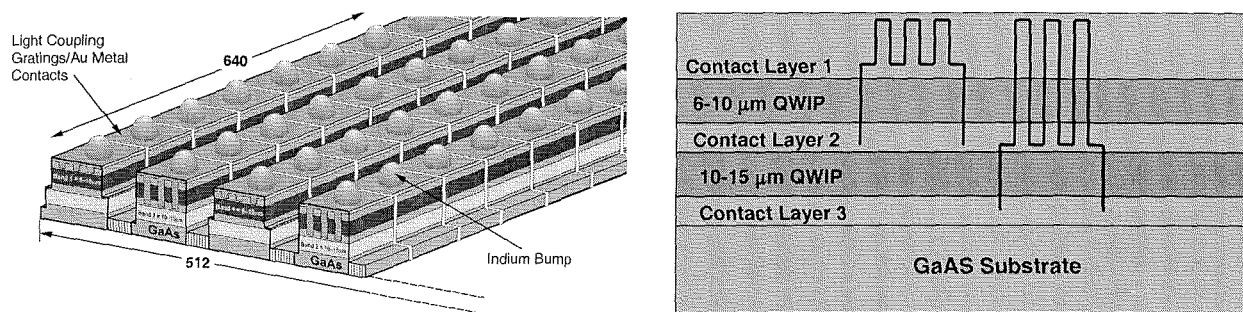


Figure 4: (Left) A schematic pixel diagram of dual broadband QWIP array. Each column represents a single band 640 pixels of the FPA. In addition to light coupling, two dimensional reflective gratings on top of the pixels serve as contacts to the active stack while shorting the unwanted top detector stacks. The unwanted bottom detector was electrically shorted through the column from the outside of the array. (Right) A schematic device layer diagram of a dual broadband QWIP structure. Groove depths of 2-D gratings associated with the detectors are also shown in the diagram.

Figure 4 (right) shows a schematic of the layer structure of the dual-band QWIP. The structure consists of two QWIP stacks, each separated by contact layers sandwiched between the two outermost contact layers. The thickness of each QWIP stack is determined by the width of the quantum well, width of the barrier, number of periods in the MQW, and the contact-layer thickness. Usually, these thicknesses, together with well-doping densities, are calculated to optimize device performances without any external constraints [3,4,15,16]. However, in the current dual-band structure, the groove depth of the grating, which couples light to bottom QWIP stack, limits the thicknesses of the top QWIP stack. As shown in the Figure 4, the total thickness of the top QWIP stack is equal to the grating groove depth of the bottom detector. These thickness constraints are essential for obtaining a nearly flat ($< 1 \mu\text{m}$ variation) top surface across the detector array, thus ensuring successful hybridization with the readout multiplexer via indium bump-bonding [5-7].

A typical QWIP consists of a 50-period MQW structure of GaAs quantum wells, separated by $\text{Al}_x\text{Ga}_{1-x}\text{As}$ barriers, sandwiched between two GaAs contact layers [3-5]. Both GaAs contact layers and GaAs quantum well layers are doped with Si (n-type) in order to provide carriers for photoexcitation [3-5]. The QWIP detection mechanism involves photoexcitation of electrons between the ground and the first excited states of quantum wells in MQW structure. In order to optimize the performance, MQW structures are designed by placing the first excited state exactly at the well top, which is referred as a bound-to-quasibound quantum well [3-5]. The typical, spectral response of a bound to quasibound QWIP detector tuned to a specific narrowband pass ($\Delta\lambda/\lambda_p \sim 10\%$) is primarily determined by the energy width of the excited state of quantum wells [3-5]. A broadband MQW structure can be designed by including units of several quantum wells with slightly different parameters such as well width and barrier height [10]. Since each single set of parameters for a quantum well corresponds to a narrow spectral bandpass of about $\Delta\lambda/\lambda_p \sim 10\%$, two or more different sets of values are sufficient to cover a broader spectral region [10].

4. DUAL BROADBAND DETECTOR

One of the critical requirements of the current FPA is minimal overlap between two spectra to avoid aliasing near the Nyquist folding wavelength [1,2]. The traditional broadband design involved a few-period-superlattice in place of each quantum well of the MQW structure [10]. Spectral broadening occurs due to overlap of the wave functions associated with excited states of the superlattice, where the quantum wells are separated by thin barriers. Although this design shows a smoother broadband spectrum, spectral fall-off and bandwidth are very sensitive for the superlattice parameters, i.e., well width and barrier thickness. The spectrum also contains a longer spectral tail towards the shorter wavelengths due to transitions associated with continuum minibands. Therefore, we use new "intermixed" broadband QWIP that consist of MQW structure with alternatively placed two types of quantum wells designed to operate at different peak wavelengths with the broad spectral band. These intermixed designs show double narrowband peaks and sharper spectral fall-offs which are easily controllable within the broad spectral band.

During the design, the bottom, longer wavelength QWIP device structure was optimized to minimize the dark current. This dark current is the highest among the two detectors because its smallest subband gap is associated with the longest-wavelength response [3-5]. Due to thickness restrictions set by the optical gratings, a lower number of periods and thinner barriers were used in the top QWIP. In order to balance the lowered absorption quantum efficiency associated with fewer periods, quantum wells are doped to a higher carrier density [15]. Typically, this is not the preferred way to improve QWIP performance because higher carrier density increases the thermal excitation (i.e., dark current) of the detector. However, this not a problem for the top detector of the dual band structure, because it operates at a lower temperature, which is set by the longest wavelength detector. The actual device contains two stacks of an 15-period 0.8 μm -thick, and a 20-period 2.3 μm -thick, broadband MQW structures. The quantum well parameters of top and bottom detectors were designed to respond at 6-9.5 μm and 10-14.5 μm wavelengths respectively. Photosensitive MQW stacks were separated by a heavily doped intermediate GaAs contact layer, with a 0.6 μm thickness (see Figure 1). The top and bottom quantum wells in the structures are doped with Si up to a carrier density of $n = 6 \times 10^{17} \text{ cm}^{-3}$ and $n = 2 \times 10^{17} \text{ cm}^{-3}$ respectively. This whole dual-band QWIP device structure is then sandwiched between the 1.35 μm top and 1.0 μm bottom GaAs contact layers doped with $n \sim 6 \times 10^{17} \text{ cm}^{-3}$.

5. DETECTOR PERFORMANCE

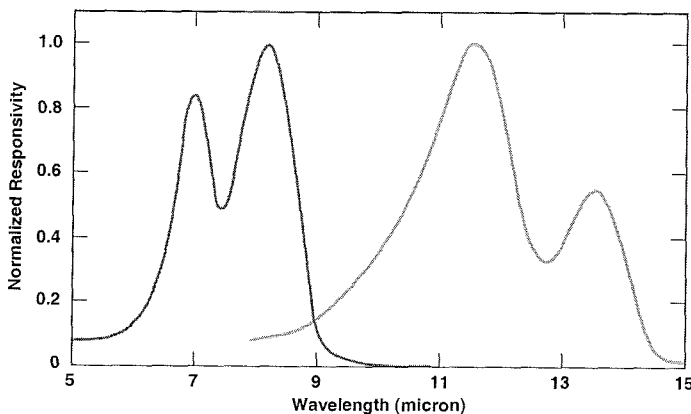


Figure 5: Normalized spectral responsivity of the test detectors in the dual broadband QWIP. Both detectors show double peaks due to use of "intermixed" MQW design. The center dip in the spectra can be smoothed by carefully optimizing the light coupling grating associated with each detector

The sample was grown by molecular beam epitaxy on a 3" semi-insulating GaAs substrate wafer. In order to characterize the device, large test mesas, 200 μm to 400 μm in diameter, were fabricated using wet chemical etching and evaporation of Au/Ge ohmic contacts on the top and bottom contact layers [3-5]. The responsivity spectra of these detectors were measured using a 1000-K blackbody source and a grating monochromator. The detectors were back illuminated through a 45-deg. polished facet to obtain normalized responsivity spectra at different bias voltages [3-5].

The source wavelength should

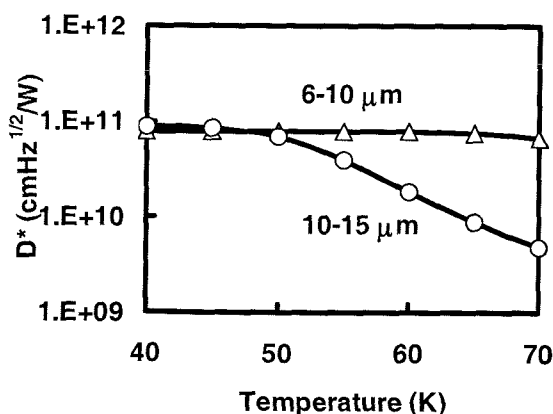


Figure 7: Detectivity (D^*) at $V_B = -1.0 \text{ V}$ versus Temperature (K). The nearly flat curves at lower temperatures suggest background-limited operating conditions.

temperatures $T > 50 \text{ K}$.

wavelength detector shows the higher dark current level. Expected pixel level photocurrents for 300 K background with $f/2$ optics were obtained from measured spectral responsivities and plotted in the same figure for comparison. Using experimental measurements of responsivity and dark current, one can now calculate the specific detectivity D^* from $D^* = R\sqrt{A\Delta B} / i_n$, where R is the responsivity, A is the detector area, ΔB is the frequency bandwidth, and $i_n = \sqrt{4eI_T g_n \Delta B}$ is the shot noise current [3-5]. Here, I_T is the total current through the detector and g_n is the noise gain. It is a good approximation when using QWIP technology to assume that the noise gain is equal to the photoconductive gain, g_p (usually, $g_p \geq g_n$), which can be easily obtained by measuring responsivity and absorption quantum efficiency [3-5,18,19]. Figure 7 shows calculated D^* values at different temperatures for all four detectors. The nearly flat curves at lower temperatures suggests background-limited operating conditions. For imaging, the detector array can be operated at temperature $T = 50$ K, where the photocurrents are higher than the dark currents, and each detector shows a very high $D^* \sim 1 \times 10^{11} \text{ cm}\sqrt{\text{Hz}}/\text{W}$ for 300-K background with $f/2$ optics. Figure 8 shows the estimated noise-equivalent temperature difference (NEAT) for each FPA band as a function of operating temperature.

6. SUMMARY

In summary, a 512×640 format, dual broadband, QWIP FPA is being developed for an imaging interferometer. This is a new type of imaging interferometer which is based on special Fourier-transform spectroscopy, scans interferograms digitally without moving any optical components. It is stable enough to measure fluctuating target signatures from unstable platforms, making it ideal for detecting chemical agents from a remotely piloted aircraft. These static interferometers require large-format FPAs with high uniformity and operability. QWIP technology is ideal for this instrument because it has achieved remarkable success in advancing highly uniform, highly operability, and large-format multicolor FPAs. The FPA used in the interferometer covers the wavelength from 6 -10 μm and 10 -15 μm in alternative rows.

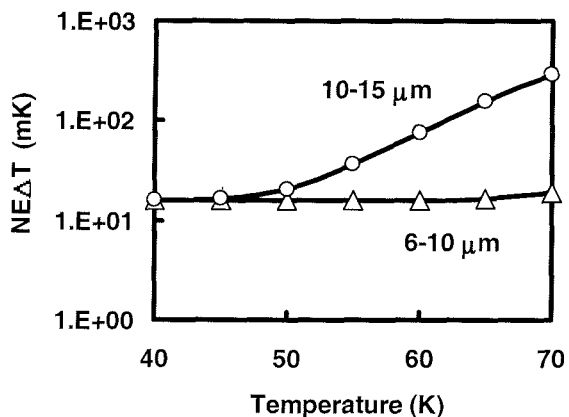


Figure 8: Noise-equivalent temperature difference (NEAT) as a function of temperature at bias voltage $V_B = -1.0$ V. NEAT is estimated for 300K background with $f/2$ optics using experimental results of the test detector.

ACKNOWLEDGMENT

The research described in this paper was carried out at the Center for Space Microelectronics Technology, Jet Propulsion Laboratory, California Institute of Technology, and was jointly sponsored by the NASA Cross Enterprise Technology Development Program and DARPA Photonic-WASSP program.

REFERENCES

1. F. M. Reininger, *Infrared Phys. & Tech.*, **42**, 345 (2001).
2. F. M. Reininger, *Spatially Modulated Interferometer for mapping Martian water vapour sources*, Ph. D. Thesis, Department of Atmospheric Physics, University of Oxford (2000).
3. B. F. Levine, *J. Appl. Phys.* **74**, R1 (1993).
4. S. D. Gunapala and S. V. Bandara, *Physics of Thin Films*, edited by M. H. Francombe and J. L. Vossen, Vol. **21**, pp. 113-237, Academic Press, NY (1995).
5. S. D. Gunapala and S. V. Bandara, *Quantum Well Infrared Photodetector (QWIP) Focal Plane Arrays, Semiconductors and Semimetals*, **62**, 197-282, Academic Press (1999).
6. S. D. Gunapala, S. V. Bandara, A. Singh, J. K. Liu, S. B. Rafol, E. M. Luong, J. M. Mumolo, N. Q. Tran, J. D. Vincent, C. A. Shott, J. Long, and P. D. LeVan, *IEEE Trans. Elec. Devices* **47**, pp. 963-971 (2000).
7. S. V. Bandara, S. D. Gunapala, J. K. Liu, S. B. Rafol, D. Z. Ting, J. M. Mumolo, F. M. Reininger, J. M. Fastenau, A. K. Liu, *SPIE* **4454**, 30 (2001).
8. S. V. Bandara, S. D. Gunapala, J. K. Liu, S. B. Rafol, J. M. Mumolo, and D. Z. Ting, "Array of QWIPs With Spatial Separation of Multiple Colors" *NASA Tech Briefs*, Vol. **26** No. 5, 8a (2002).
9. K. K. Choi, S. V. Bandara, S. D. Gunapala, W. K. Liu, and J. M. Fastenau, *J. Appl. Phys.* **91**, 5230 (2002).
10. S. V. Bandara, S. D. Gunapala, J. K. Liu, E. M. Luong, J. M. Mumolo, W. Hong, D. K. Sengupta, and M. J. McKelvey, *Appl. Phys. Lett.* **72**, 2427 (1998).
11. J. Y. Andersson, L. Lundqvist, and Z. F. Paska, *J. Appl. Phys.* **71**, 3600 (1991).
12. G. Sarusi, B. F. Levine, S. J. Pearton, S. V. Bandara, and R. E. Leibenguth, *J. Appl. Phys.* **76**, 4989 (1994).
13. G. Sarusi, S. D. Gunapala, J. S. Park, and B. F. Levine, *J. Appl. Phys.* **76**, 6001 (1994).
14. S. V. Bandara, S. D. Gunapala, J. K. Liu, W. Hong and J. S. Park, *SPIE Proceedings- IR Technology and Applications*, Vol. **3061** (1997).
15. S. D. Gunapala, B. F. Levine, L. Pfeiffer, and K. West, *J. Appl. Phys.* **69**, 6517 (1991).
16. K. K. Choi, *J. Appl. Phys.* **73**, 5230 (1993).
17. S. V. Bandara et al., U.S. Patent 6521967 (2003).
18. K. K. Choi, *J. Appl. Phys.* **80**, 1257 (1996).
19. H. C. Liu, *Appl. Phys. Lett.* **61**, 2703 (1992).